

Uncovering Ionic Transport Paths within Hierarchically Structured Battery Electrodes

Johanna Naumann,* Marcus Müller, Nicole Bohn, Joachim R. Binder, Marc Kamlah,* and Yixiang Gan

Cite This: *ACS Appl. Energy Mater.* 2024, 7, 4786–4793

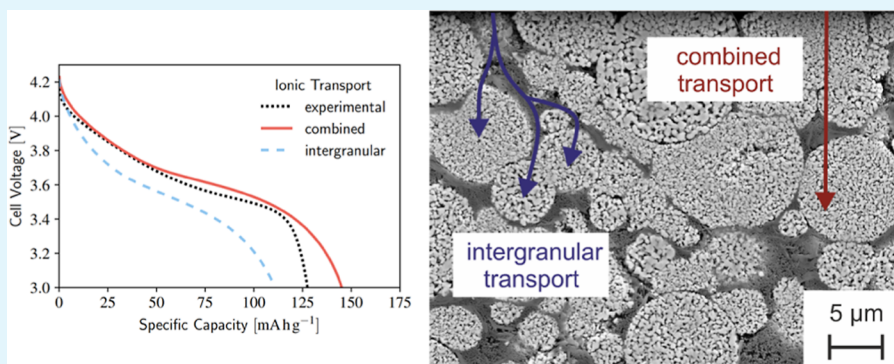
Read Online

ACCESS |

Metrics & More

Article Recommendations

Supporting Information



ABSTRACT: Calendering battery electrodes improves electronic transport and energy density while increasing the ionic resistance in the pore space. In hierarchically structured electrodes, the open porosity of the active material particles offers additional ionic transport paths. However, there is a lack of knowledge about the interaction between these pores and the porosity surrounding the particles. Considering both inter- and intragranular pore space, we combine a Doyle–Fuller–Newman cell model with experimental discharge curves to show that ionic transport paths in hierarchically structured electrodes change with compaction and the discharge rate. If the intergranular porosity is high, it carries most of the ionic current from the separator to the current collector. The intragranular porosity ensures ionic transport into the porous particles. High compaction of a hierarchically structured electrode leads to an increasing contribution of the intragranular pores to ionic transport across the electrode with a rising discharge rate. This study offers a modeling approach to explore the optimum calendering process for different types of hierarchically structured electrode materials.

KEYWORDS: electrode morphology, hierarchical porosity, porous particles, effective transport, tortuosity, intercalation battery, continuum cell model

1. INTRODUCTION

During production, granular battery electrodes are mechanically compressed. This calendering step reduces the porosity and ensures good contact among the active material, electronically conductive additives, and current collector. As a result, the volumetric energy density increases and the electronic conductivity through the electrode improves.¹ However, calendering also aggravates the resistance for ionic transport in the pore space by raising the tortuosity.²

Electrode architecture affects the ionic resistance of the battery electrodes. Examples are laser-induced grooves³ or the morphology of the active material particles.⁴ For the special case of particles which possess an open porosity, the tortuosity at a given electrode porosity is higher than in electrodes with compact particles.⁵ These hierarchically structured electrodes incorporate two classes of pores: the intragranular porosity within the particles and the intergranular porosity between the particles. The intragranular porosity enhances access to the

active material and mitigates limitations due to solid diffusion.⁶ Consequently, the specific capacity increases, especially at high insertion and extraction rates.^{7–9} Contrary to electrodes consisting of loose nanoparticles, hierarchically structured electrodes maintain access to the primary particle surfaces during cycling¹⁰ and require less carbon and binder additives.¹¹ Hierarchical electrode designs have been applied to a multitude of innovative battery technologies, including sodium,^{12,13} potassium,¹⁴ zinc,¹⁵ and lithium-sulfur¹⁶ batteries.

Calendering hierarchically structured electrodes initially reduces the intergranular pore space while the porous particles

Received: February 28, 2024

Revised: May 3, 2024

Accepted: May 6, 2024

Published: May 30, 2024



remain intact.¹¹ They may undergo a plastic-like deformation to eliminate intergranular pores while maintaining their original intragranular porosity. Schneider et al.⁵ found a strong increase in tortuosity when the intergranular porosity is eliminated at an electrode porosity of around 0.3. The small intergranular pore size causes a higher tortuosity than the large intergranular pore size at the same porosity. Below electrode porosities of 0.3, intragranular porosity may change due to massive compression⁵ or fracture.¹⁷ Despite these insights into ionic transport in hierarchically structured electrodes, the interplay of intra- and intergranular porosity during ionic transport has not yet been understood.

Multiple methods are available to model transport through a hierarchy of pores. A widely used approach is pore network models,¹⁸ which simplify a porous medium to a network of pore bodies and pore throats of different sizes capturing the relevant features of the transport. Meyers and Liapis^{19,20} developed a pore network model to study columns packed with chromatographic porous particles. Sadeghi et al.²¹ investigated the reactive transport in a hierarchically porous catalyst with a pore network model. More detailed models spatially resolve the hierarchical structure. Examples include modeling reactive transport in micro-/mesoporous materials with added macropores by the lattice Boltzmann method,²² dynamic Monte Carlo simulations of mass transfer in a network of mesopores within a microporous continuum,^{23,24} or molecular simulation of transport in different hierarchically porous structures under a pressure gradient.²⁵ Tallarek et al.²⁶ combined molecular dynamics with Brownian dynamics to derive effective diffusion coefficients in hierarchically structured materials. Gritti and Guiochon^{27,28} compared and developed several models for macroscopic sample diffusion in chromatographic columns packed with fully and superficially porous particles. However, these approaches require time-consuming model building or numerically expensive simulations. In contrast, explicit formulas for effective transport through hierarchically porous structures allow easy integration in multiphysics models. Combining the Maxwell equation and conductivity measurements, Barrande et al.²⁹ developed an explicit expression for the tortuosity of a suspension of porous particles. But this expression lacks the possibility to include additional impermeable phases like carbon additives or binder, which are used in battery electrodes.

Modeling hierarchically structured battery electrodes can predict the local change in concentration within the electrolyte over time. So far, modeling works focused on a single porous particle³⁰ or only slightly calendered electrodes.^{31,32} However, realistic applications require high compaction to achieve a sufficient energy density.⁵ Here, we present a modified continuum cell model³¹ to uncover to what extent intra- and intergranular pores contribute to the ionic transport across the electrode. It includes a newly developed explicit expression for effective ionic transport through hierarchically porous structures based on the M -factor concept.^{33,34} This expression assumes parallel ionic transport through intra- and intergranular pores. Also, we consider the simpler assumption that ionic transport mainly takes place in intergranular pores only. Comparing both assumptions in terms of the resulting salt concentration distribution in the electrolyte as well as cell performance, we will show that ionic transport paths depend on the degree of electrode compaction and on the discharge rate. With increasing compaction and rates, the ionic transport direction in intragranular pores shifts from transport into the

particles to transport through the particles. Therefore, the intragranular porosity contributes to the ionic transport across highly calendered electrodes, which has to be taken into account in cell models.

2. METHODS

We employed a Doyle–Fuller–Newman cell model for hierarchically structured electrodes.³¹ Concerning ionic transport from the separator to the current collector (coordinate x), the model describes conservation of ionic mass (concentration \bar{c}_e) and charge (electrochemical potential $\bar{\phi}_e$) in the electrolyte of volume fraction ε_e over time t by

$$\varepsilon_e \frac{\partial \bar{c}_e}{\partial t} = \frac{\partial}{\partial x} \left(D_{e,\text{eff}} \frac{\partial \bar{c}_e}{\partial x} \right) + \varepsilon_s \bar{j}_m \quad (1)$$

$$\frac{\partial}{\partial x} \left(\kappa_{e,\text{eff}} \frac{\partial \bar{\phi}_e}{\partial x} + \kappa_{D,\text{eff}} \frac{\partial \ln \bar{c}_e}{\partial x} \right) = -\varepsilon_s \bar{j}_{\text{ch}} \quad (2)$$

Ions may leave this path by transport into the spherically symmetric and porous active material particles, which is accounted for by the sink terms $\varepsilon_s \bar{j}_m$ and $-\varepsilon_s \bar{j}_{\text{ch}}$. The effective diffusivity $D_{e,\text{eff}}$, the effective conductivity $\kappa_{e,\text{eff}}$ and the effective diffusional conductivity $\kappa_{D,\text{eff}}$ of the electrolyte determine the magnitude of effective ionic transport. The original model assumes effective ionic transport from the separator to

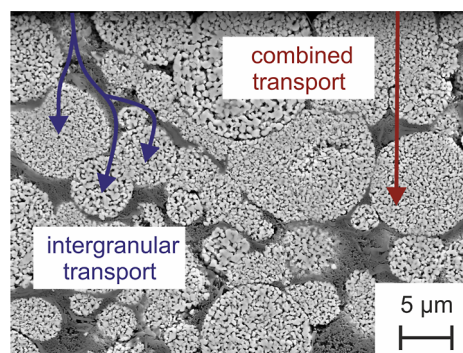


Figure 1. Schematic of possible ionic transport paths across the electrode thickness: main ionic transport through intergranular pores (intergranular transport) or significant contribution by intragranular pores (combined transport).

the current collector in the intergranular pores (Figure 1, intergranular transport) in the form

$$D_{\text{eff}} = M^{\text{inter}} D \quad (3)$$

with M -factor M^{inter} , which reduces the bulk property D according to the intergranular pore network. This purely intergranular transport occurs when all of the ions entering the porous particles are consumed by the electrochemical intercalation reaction on the way inside. If the ionic current exceeds this amount, part of the ions will travel through the particles and contribute to the overall ionic current from the separator to the current collector. This additional transport path will decrease the ionic resistance of the electrode. Therefore, we assumed parallel transport through the porous particles and through the intergranular pores (Figure 1, combined transport)

$$D_{\text{eff}} = M^{\text{combi}} D = (M^{\text{inter}} + M^{\text{intra}}) D \quad (4)$$

with M -factor M^{combi} for a combined intra- plus intergranular ionic transport. The partial M -factor M^{intra} describes the effective ionic transport through the network of porous particles, which depends on two factors. First, the intragranular pore network possesses an intrinsic tortuosity described by the M -factor M^{II} . Due to the small

intragranular pore size, M^{II} is lower than M^{inter} at the same porosity (Section S2). Second, bottlenecks at the contact regions of two porous particles will further reduce the effective ionic transport through the particle network. The M -factor of interconnected spherical particles of the same size follows the fit formula³⁵

$$M^{\text{particles}} = (\varepsilon_s^{\text{pos}} - 0.62)^{0.8015 + \frac{0.3227}{\theta} - \frac{13.88}{47.37 - \theta}} \quad (5)$$

with volume fraction $\varepsilon_s^{\text{pos}}$ of the particles and percolation threshold 0.62. The mean contact angle θ can be calculated via the fit formula³⁵

$$\theta = \frac{\ln\left(\frac{15.625}{1 - \varepsilon_s^{\text{pos}}} - 43.277\right)}{0.166} \quad (6)$$

For $\theta < 0$, $M^{\text{particles}}$ is set to zero since there is no percolation among the particles. Combining all partial M -factors yields the overall M -factor for intra- plus intergranular transport

$$M^{\text{combi}} = M^{\text{inter}} + M^{\text{particles}} M^{\text{II}} \quad (7)$$

We applied eqs 4 and 7 to all effective ionic transport properties $D_{e,\text{eff}}$, $\kappa_{e,\text{eff}}$, and $\kappa_{D,\text{eff}}$ in the model (eqs 1 and 2).

We accounted for a changing contact resistance between the electrode and current collector⁵ during calendaring, which contributed to a decrease in electrode resistivity¹¹ (Table 1). The contact resistance R_{cont} leads to a potential drop at the interface depending on the applied current i_{app}

$$\Delta\phi_s = R_{\text{cont}} i_{\text{app}} \quad (8)$$

which affects the acquired cell voltage (Figure 2).

Table 1. Electrode Characteristics at Different Calendaring Steps^{5,11}

calendaring	uncalendered	Cal-1	Cal-2	Cal-3
electrode thickness L^{pos} [μm]	89	69	57	52
intergranular porosity $\varepsilon_e^{\text{pos}}$ [-]	0.435	0.271	0.118	0.032
volume fraction of porous particles $\varepsilon_s^{\text{pos}}$ [-]	0.487	0.628	0.760	0.834
volume fraction of NMC111 $\varepsilon_s^{\text{pos}} \varepsilon_s^{(\text{II})}$ [-]	0.272	0.351	0.424	0.465
volume fraction of additives $\varepsilon_f^{\text{pos}}$ [-]	0.078	0.101	0.122	0.134
total porosity $\varepsilon_e^{\text{pos}} + \varepsilon_s^{\text{pos}} \varepsilon_s^{(\text{II})}$ [-]	0.650	0.548	0.454	0.401
contact resistance R_{cont} [$\Omega \text{ m}^2$]	0.0060	0.0020	0.0010	0.0008
total resistivity R [$\Omega \text{ m}$]	50	8	5	4

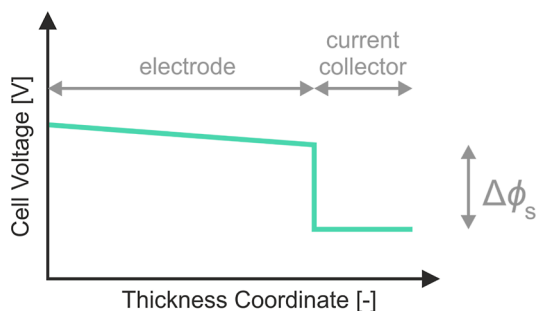


Figure 2. Schematic of electronic potential over cell thickness with potential drop due to contact resistance between the electrode and current collector.

The diffusivity of lithium ions in the considered active material $\text{LiNi}_{1/3}\text{Mn}_{1/3}\text{Co}_{1/3}\text{O}_2$ (NMC111) changes around 1.5 orders of

magnitude depending on the degree of lithiation l .³⁶ We employed a piecewise fit

$$D_s[\text{m}^2\text{s}^{-1}] = \begin{cases} 10^{-a} & l \leq 0.5 \\ 10^{-7.5l+3.75-a} & 0.5 < l < 0.7 \\ 10^{-1.5-a} & l \geq 0.7 \end{cases} \quad (9)$$

with a fitting parameter a to account for the variation.

We studied hierarchically structured electrodes, which contained modified NM-3100 (NMC111) by Toda Kogyo Corp., C-ENERGY Super C65 (carbon black) and C-ENERGY KS6L (graphite) by Imerys Graphite & Carbon, Switzerland, and Solef 5130 (PVDF binder) by Solvay S.A. The total solid content in the slurry amounted to 20.4 vol % with a $3.3 \text{ m}^2 \text{ g}^{-1}$ BET surface area¹¹ of the active material powder. Previous publications report detailed experimental characterization and synthesis of the electrodes¹¹ as well as electrodes with a similar active material.^{5,9} After coating and drying, the electrodes were calendered to three different porosities (Cal-1, Cal-2, and Cal-3). When calendaring hierarchically structured electrodes to electrode porosities above 0.3, the intergranular porosity reduces while the particles stay intact.¹¹ Particles may even undergo plastic-like deformation without disintegrating. Only after eliminating most of the intergranular porosity, the intragranular porosity decreases with further compaction.⁵ Therefore, we assumed that the intragranular porosity $\varepsilon_e^{(\text{II})}$ for all calendered electrodes remains constant at 0.442, which is the intergranular porosity of the active material powder.¹¹ From the mass and size of the electrodes as well as the densities of active material and additives, we calculated the volume fractions of intergranular pores, porous particles, and additives (Table 1). Section S2 lists further properties of the investigated cells. Upon cycling, NMC111 undergoes very little volume change. When lithium atoms intercalate in the crystal structure, the a -lattice expands. At the same time, the c -lattice shrinks due to electrostatic repulsion of the oxygen layers.³⁷ This anisotropic behavior results in a volume change of no more than 1%.^{38–40} Therefore, we could assume that the volume fractions remained constant during cell discharge.

The hierarchically structured cell model with both assumptions for ionic transport was fitted to experimental discharge curves of the slightly calendered electrode Cal-1 at 1 C and 7 C (Figure 3). For $a = 14.4$ (eq 9) and an active material electronic conductivity of $\sigma^{(\text{II})} = 3 \cdot 10^{-5} \text{ S m}^{-1}$, the models yielded results similar to those of the experiment. The values of the two fitting parameters comply with measurements of the diffusivity⁴¹ and electronic conductivity⁴² of NMC111. The models reproduced the beginning of the 1 C discharge and the entire 7 C discharge. However, for the 1 C discharge, they overestimated the specific capacity of the cell. Overall, we found the model to be suitable to describe the electrochemical processes within the hierarchically structured electrode.

3. RESULTS AND DISCUSSION

The M -factor M^{combi} (eq 7) for combined intra- plus intergranular ionic transport varies with intergranular porosity during calendaring (Figure 4). Part of this results from the partial M -factor M^{inter} of the intergranular pore network, which depends on the amount of available porosity. Above an intergranular porosity of 0.245, the network of porous particles shows no percolation. Therefore, the partial M -factor $M^{\text{particles}}$ is zero, and both assumptions for ionic transport yield the same overall M -factor. Below the intergranular porosity of 0.245, the intergranular porosity also influences the intragranular portion of the M -factor. Calendaring increases the volume fraction and interconnectedness of the porous particles in the electrode. Therefore, the M -factor $M^{\text{particles}}$ rises with decreasing intergranular porosity. As a result, the effective combined intra- plus intergranular ionic transport yields an increasingly higher M -factor than the purely intergranular assumption. The intragranular pores carry a higher fraction of the ionic current

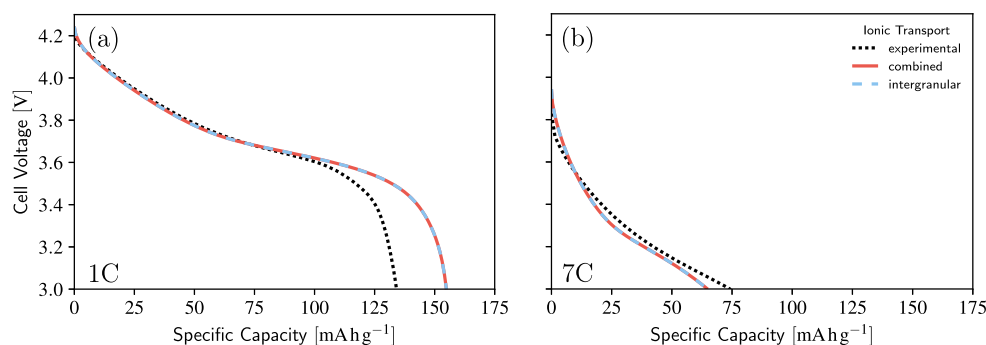


Figure 3. Comparison between experimental and modeled discharge curves of electrode Cal-1 at (a) 1 C and (b) 7 C.

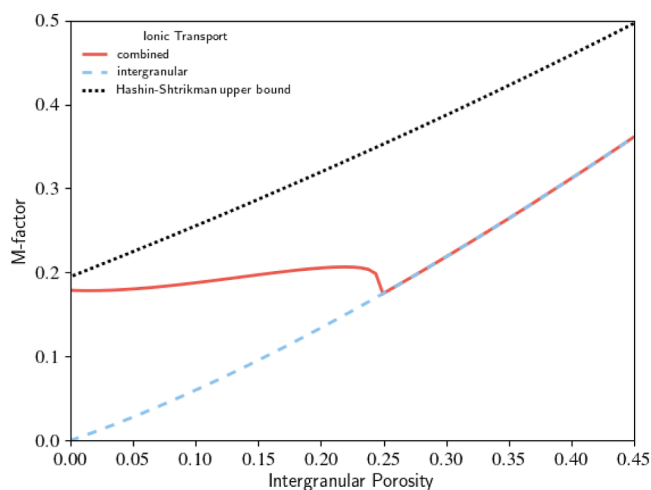


Figure 4. M -factors M^{inter} and M^{combi} for ionic transport at the cell level.

with decreasing intergranular porosity. Upon complete elimination of the intergranular porosity, when the purely intergranular assumption yields zero effective ionic transport, an M -factor of 0.19 remains for the realistic assumption of combined intra- plus intergranular transport. This is close to the Hashin–Shtrikman upper bound for material properties of multiphase systems⁴³ (details in Section S1).

With an intergranular porosity of 0.2648, electrode Cal-1 experiences the same effective ionic transport for both purely intergranular and the combined intra- plus intergranular assumption (Figure 4). Ionic transport properties of the electrode directly correlate with salt concentration profiles in the electrolyte, where good ionic transport leads to a high salt

concentration with little gradient across the electrode thickness. Consequently, there was no difference in electrolyte salt concentration between the two assumptions even at a high discharge rate of 10 C (Figure 5a). Ionic transport from the separator to the current collector takes place in the intergranular pores of electrode Cal-1. The equality of effective ionic transport also leads to the same discharge curves (Figure 5b) for both assumptions. Section S3 provides the results for all three electrodes at all investigated discharge rates.

Electrode Cal-2 with a higher degree of compaction developed lower electrolyte salt concentrations compared with electrode Cal-1. This effect can be attributed to the decrease in effective ionic transport during calendaring, since a thinner electrode without compaction would typically lead to a more even salt concentration profile and therefore to a mitigation of ionic transport limitations.³² Furthermore, electrode Cal-2 experiences a difference between the two assumptions for ionic transport (Figure 6). Already at a 1 C discharge, the purely intergranular assumption considerably underestimated the salt concentration in the electrode compared with the combined intra- plus intergranular assumption (Figure 6b). Faster discharge of 3 C (Figure 6c) and 5 C (Figure 6d) leads to large differences in electrolyte salt concentration. With an intergranular porosity of 0.1100 (Table 1), we expect combined intra-plus intergranular transport at high discharge rates (Figure 4) for electrode Cal-2. The decreasing intergranular porosity forces more ions to travel through porous particles, so a certain amount of them cross particles without being intercalated into the active material and are available for intercalation in subsequent active material particles.

Further compaction of the electrode extended the observed trend of a higher portion of intragranular ionic transport with a

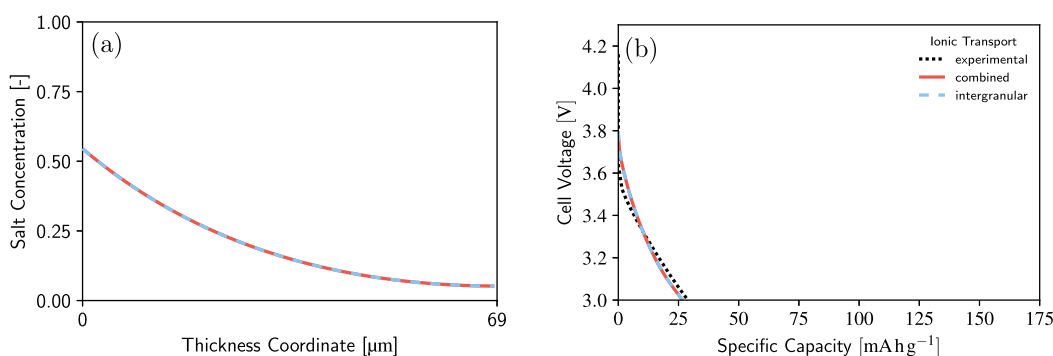


Figure 5. (a) Salt concentration in the electrolyte and (b) discharge curve of electrode Cal-1 at the end of a 10 C discharge.

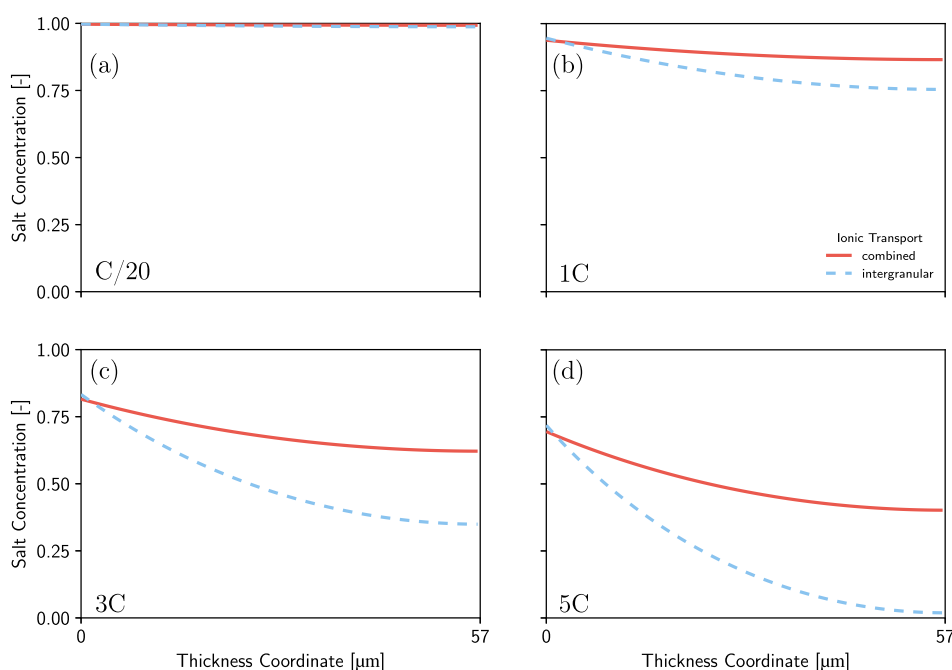


Figure 6. Salt concentration in the electrolyte of electrode Cal-2 at the end of a (a) C/20, (b) 1 C, (c) 3 C, and (d) 5 C discharge.

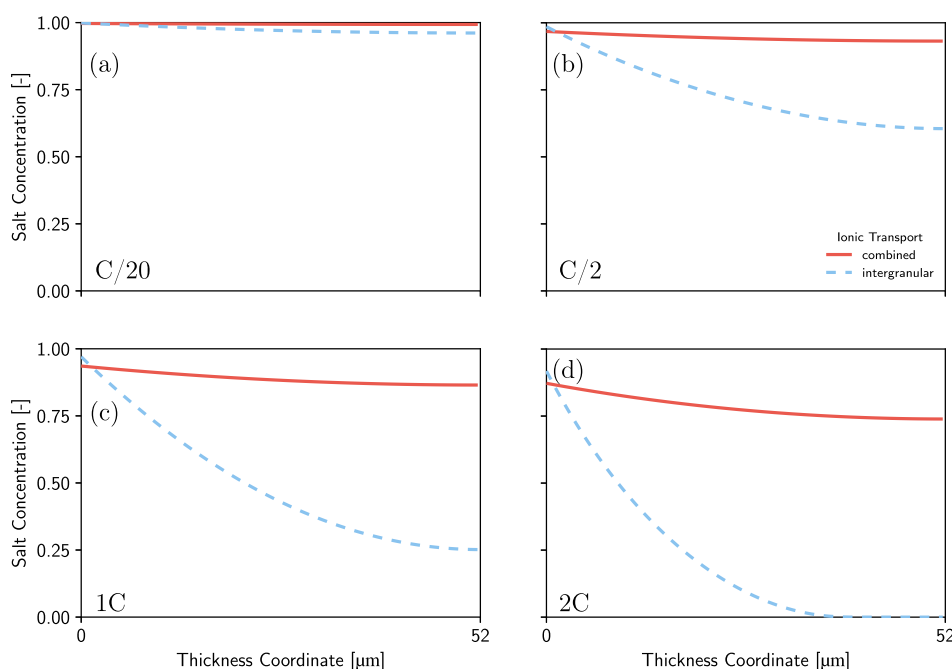


Figure 7. Salt concentration in the electrolyte of electrode Cal-3 at the end of a (a) C/20, (b) C/2, (c) 1 C, and (d) 2 C discharge.

Table 2. Gravimetric Energy Density [W h kg^{-1}] (and Deviation Compared to the Experiment) Depending on the Assumption for Ionic Transport

electrode	discharge rate	experiment	intragranular + intergranular	intergranular
Cal-2	3 C	449	472 (+5%)	462 (+3%)
Cal-2	5 C	402	361 (−10%)	326 (−19%)
Cal-3	C/2	535	593 (+11%)	589 (+10%)
Cal-3	2 C	464	529 (+14%)	393 (−15%)

rising C-rate and compaction. For electrode Cal-3, the combined intra- plus intergranular assumption yielded a more homogeneous salt concentration across the cell and thus a higher salt concentration in the positive electrode

region, compared to the purely intergranular assumption. Already at C/2, the purely intergranular assumption strongly deviated from the combined intra- plus intergranular assumption (Figure 7b). Even at this low discharge rate, the

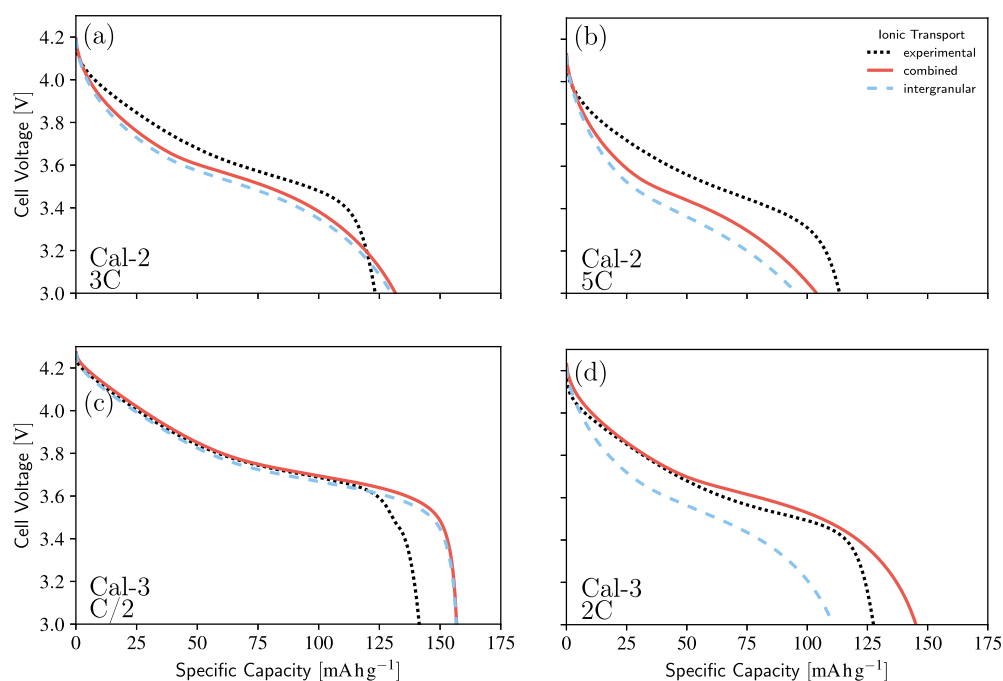


Figure 8. Discharge curve of electrode Cal-2 at (a) 3 C and (b) 5 C and electrode Cal-3 at (c) C/2 and (d) 2 C.

intragranular pores contribute significantly to the ionic current from the separator to the current collector. Intermediate discharge rates of 1 C (Figure 7c) and 2 C (Figure 7d) showed an extreme difference between the two assumptions for the ionic transport, which indicates that a large portion of ionic current moves through the intragranular pores. The intragranular porosity dominates the effective ionic transport because of the low intergranular porosity of 0.0244 (Table 1 and Figure 4).

Up to intermediate discharge rates, both assumptions for the ionic transport yielded similar energy densities of electrode Cal-2 compared with the experiment. At 3 C, the deviation lay below 5% (Table 2). The purely intergranular prediction of the discharge curve only showed a slightly lower cell voltage than the combined intra- plus intergranular prediction (Figure 8a). The energy density obtained by the purely intergranular assumptions became unrealistic at 5 C when the model predicted partial salt depletion of the electrolyte (Figure 6d). This causes the intercalation to come to a halt, yielding a significantly different discharge curve compared to the experiment (Figure 8b) with a 19% deviation in energy density (Table 2). Assuming combined intra- plus intergranular transport better predicted the experimental discharge curve with only 10% deviation in energy density.

The discharge curve of electrode Cal-3 at 2 C resulting from the purely intergranular assumption had no similarity to the experimental results, while the combined intra- plus intergranular assumption closely matched them (Figure 8d). When determining the energy density, the purely intergranular assumption underestimated the experimental value at 2 C by 15% (Table 2). Up to a C/2 discharge, both assumptions yielded a higher energy density compared to the experiment (Figure 8c) due to the tendency of the models to overestimate the specific capacity at intermediate discharge rates (compare Section 2). Again, the deviation of the modeled discharge curve and the underestimation of energy density occurred when the purely intergranular assumption led to salt depletion

of the electrolyte in regions close to the current collector (Figure 7d).

The assumption of combined intra- plus intergranular ionic transport is essential to accurately predict the discharge behavior of hierarchically structured electrodes at a high compaction and high discharge rate. In these cases, the purely intergranular assumption severely underestimates the effective ionic transport from the separator to the current collector, which results in an unrealistically low rate of intercalation. Slow discharge may lead to the same prediction of discharge curves and energy density for both assumptions, even though they result in different profiles of the electrolyte salt concentration. Salt concentration is more sensitive to effective ionic transport than the observed discharge behavior. If the intergranular porosity lies above 0.245, then ionic transport from the separator to the current collector takes place in the intergranular pores, so the purely intergranular assumption correctly predicts the discharge behavior of the cell.

4. CONCLUSIONS

In this article, we aimed to elucidate ionic transport paths in hierarchically structured electrodes. We found that there are different scenarios, depending on the discharge rate and the intergranular porosity of the electrode. In electrodes with a high intergranular porosity, the ionic current from the separator to the current collector mainly takes place in these pores. The porosity within the particles transports only the ions from the intergranular pores to the particle centers, while they are successively consumed on the way by intercalation into the active material. Calendered electrodes with a reduced intergranular porosity display this behavior only at low discharge rates. Increasing the discharge rate leads to a transition from the purely intergranular transport mode to combined intra- plus intergranular ionic transport across the electrode. Highly calendered electrodes experience this transition at lower discharge rates. For calendered hierarchically structured electrodes, continuum cell models have to

account for the ionic transport through porous particles to accurately predict the cell performance, in particular at high levels of calendaring and high discharge rates. The presented approach enables a realistic prediction of cell performance close to the optimal degree of calendaring.

■ ASSOCIATED CONTENT

SI Supporting Information

The Supporting Information is available free of charge at <https://pubs.acs.org/doi/10.1021/acsaem.4c00505>.

Calculation of Hashin–Shtrikman bound, parameters for the cell simulations, and simulation results for additional discharge rates (PDF)

■ AUTHOR INFORMATION

Corresponding Authors

Johanna Naumann – Institute for Applied Materials, Karlsruhe Institute of Technology, D-76344 Eggenstein-Leopoldshafen, Germany; orcid.org/0009-0006-0927-9564; Email: johanna.naumann@kit.edu

Marc Kamlah – Institute for Applied Materials, Karlsruhe Institute of Technology, D-76344 Eggenstein-Leopoldshafen, Germany; Email: marc.kamlah@kit.edu

Authors

Marc Müller – Institute for Applied Materials, Karlsruhe Institute of Technology, D-76344 Eggenstein-Leopoldshafen, Germany; orcid.org/0000-0002-5562-7201

Nicole Bohn – Institute for Applied Materials, Karlsruhe Institute of Technology, D-76344 Eggenstein-Leopoldshafen, Germany

Joachim R. Binder – Institute for Applied Materials, Karlsruhe Institute of Technology, D-76344 Eggenstein-Leopoldshafen, Germany; orcid.org/0000-0003-2237-1411

Yixiang Gan – School of Civil Engineering and The University of Sydney Nano Institute, The University of Sydney, Camperdown, New South Wales 2006, Australia; orcid.org/0000-0002-9621-0277

Complete contact information is available at: <https://pubs.acs.org/doi/10.1021/acsaem.4c00505>

Notes

The authors declare no competing financial interest.

■ ACKNOWLEDGMENTS

This work contributes to the research performed at CELEST (Center for Electrochemical Energy Storage Ulm-Karlsruhe) and was funded by the German Research Foundation (DFG) under Project ID 390874152 (POLiS Cluster of Excellence, EXC 2154). We thank the Ministry of Science, Research and Arts Baden-Württemberg, for financial support.

■ REFERENCES

- (1) Abdollahifar, M.; Cavers, H.; Scheffler, S.; Diener, A.; Lippke, M.; Kwade, A. Insights into Influencing Electrode Calendaring on the Battery Performance. *Adv. Energy Mater.* **2023**, *13*, 2300973.
- (2) Shodiev, A.; Chouchane, M.; Gaberscek, M.; Arcelus, O.; Xu, J.; Oularbi, H.; Yu, J.; Li, J.; Morcrette, M.; Franco, A. A. Deconvoluting the Benefits of Porosity Distribution in Layered Electrodes on the Electrochemical Performance of Li-Ion Batteries. *Energy Storage Mater.* **2022**, *47*, 462–471.
- (3) Song, Z.; Zhu, P.; Pflöging, W.; Sun, J. Electrochemical Performance of Thick-Film $\text{Li}(\text{Ni}_{0.6}\text{Mn}_{0.2}\text{Co}_{0.2})\text{O}_2$ Cathode with Hierarchical Structures and Laser Ablation. *Nanomaterials* **2021**, *11*, 2962.
- (4) Landesfeind, J.; Hattendorff, J.; Ehrl, A.; Wall, W. A.; Gasteiger, H. A. Tortuosity Determination of Battery Electrodes and Separators by Impedance Spectroscopy. *J. Electrochem. Soc.* **2016**, *163*, A1373–A1387.
- (5) Schneider, L.; Klemens, J.; Herbst, E. C.; Müller, M.; Scharfer, P.; Schabel, W.; Bauer, W.; Ehrenberg, H. Transport Properties in Electrodes for Lithium-Ion Batteries: Comparison of Compact versus Porous NCM Particles. *J. Electrochem. Soc.* **2022**, *169*, 100553.
- (6) Cabelguen, P.-E.; Peralta, D.; Cugnet, M.; Maillot, P. Impact of Morphological Changes of $\text{LiNi}_{1/3}\text{Mn}_{1/3}\text{Co}_{1/3}\text{O}_2$ on Lithium-Ion Cathode Performances. *J. Power Sources* **2017**, *346*, 13–23.
- (7) Li, L.; Wang, L.; Zhang, X.; Xie, M.; Wu, F.; Chen, R. Structural and Electrochemical Study of Hierarchical $\text{LiNi}_{1/3}\text{Co}_{1/3}\text{Mn}_{1/3}\text{O}_2$ Cathode Material for Lithium-Ion Batteries. *ACS Appl. Mater. Interfaces* **2015**, *7*, 21939–21947.
- (8) Chen, Z.; Wang, J.; Chao, D.; Baikie, T.; Bai, L.; Chen, S.; Zhao, Y.; Sum, T. C.; Lin, J.; Shen, Z. Hierarchical Porous $\text{LiNi}_{1/3}\text{Co}_{1/3}\text{Mn}_{1/3}\text{O}_2$ Nano-/Micro Spherical Cathode Material: Minimized Cation Mixing and Improved Li^+ Mobility for Enhanced Electrochemical Performance. *Sci. Rep.* **2016**, *6*, 25771.
- (9) Wagner, A. C.; Bohn, N.; Geßwein, H.; Neumann, M.; Osenberg, M.; Hilger, A.; Manke, I.; Schmidt, V.; Binder, J. R. Hierarchical Structuring of NMC111-Cathode Materials in Lithium-Ion Batteries: An In-Depth Study on the Influence of Primary and Secondary Particle Sizes on Electrochemical Performance. *ACS Appl. Energy Mater.* **2020**, *3*, 12565–12574.
- (10) Zhou, L.; Zhang, K.; Hu, Z.; Tao, Z.; Mai, L.; Kang, Y.-M.; Chou, S.-L.; Chen, J. Recent Developments on and Prospects for Electrode Materials with Hierarchical Structures for Lithium-Ion Batteries. *Adv. Energy Mater.* **2018**, *8*, 1701415.
- (11) Müller, M.; Schneider, L.; Bohn, N.; Binder, J. R.; Bauer, W. Effect of Nanostructured and Open-Porous Particle Morphology on Electrode Processing and Electrochemical Performance of Li-Ion Batteries. *ACS Appl. Energy Mater.* **2021**, *4*, 1993–2003.
- (12) Häring, M.; Geßwein, H.; Bohn, N.; Ehrenberg, H.; Binder, J. R. Influence of Process Parameters on the Electrochemical Properties of Hierarchically Structured $\text{Na}_3\text{V}_2(\text{PO}_4)_3/\text{C}$ Composites. *ChemElectroChem* **2024**, *11*, No. e202300401.
- (13) Schmidt, M.; Mereacre, V.; Geßwein, H.; Bohn, N.; Indris, S.; Binder, J. R. High Performance of Porous, Hierarchically Structured $\text{P2-Na}_{0.6}\text{Al}_{0.11-x}\text{Ni}_{0.22-y}\text{Fe}_{x+y}\text{Mn}_{0.66}\text{O}_2$ Cathode Materials. *Adv. Energy Mater.* **2024**, 2301854.
- (14) Weng, J.; Duan, J.; Sun, C.; Liu, P.; Li, A.; Zhou, P.; Zhou, J. Construction of Hierarchical $\text{K}_{0.7}\text{Mn}_{0.7}\text{Mg}_{0.3}\text{O}_2$ Microparticles as High Capacity & Long Cycle Life Cathode Materials for Low-Cost Potassium-Ion Batteries. *Chem. Eng. J.* **2020**, *392*, 123649.
- (15) Wu, X.; Yin, C.; Zhang, M.; Xie, Y.; Hu, J.; Long, R.; Wu, X.; Wu, X. The Intercalation Cathode of MOFs-Driven Vanadium-Based Composite Embedded in N-Doped Carbon for Aqueous Zinc Ion Batteries. *Chem. Eng. J.* **2023**, *452*, 139573.
- (16) Li, L.; Du, X.; Liu, G.; Zhang, Y.; Zhang, Z.; Li, J. Micro-/Mesoporous Co-NC Embedded Three-Dimensional Ordered Macroporous Metal Framework as Li-S Battery Cathode towards Effective Polysulfide Catalysis and Retention. *J. Alloys Compd.* **2022**, *893*, 162327.
- (17) Tao, R.; Steinhoff, B.; Uzun, K.; La Riviere, B.; Sardo, K.; Skelly, B.; Hill, R.; Cheng, Y.-T.; Li, J. Correlation among Porosity, Mechanical Properties, Morphology, Electronic Conductivity and Electrochemical Kinetics of Dry-Processed Electrodes. *J. Power Sources* **2023**, *581*, 233481.
- (18) Xiong, Q.; Baychev, T. G.; Jivkov, A. P. Review of Pore Network Modelling of Porous Media: Experimental Characterisations, Network Constructions and Applications to Reactive Transport. *J. Contam. Hydrol.* **2016**, *192*, 101–117.

- (19) Meyers, J. J.; Liapis, A. I. Network Modeling of the Intraparticle Convection and Diffusion of Molecules in Porous Particles Packed in a Chromatographic Column. *J. Chromatogr. A* **1998**, *827*, 197–213.
- (20) Meyers, J. J.; Liapis, A. I. Network Modeling of the Convective Flow and Diffusion of Molecules Adsorbing in Monoliths and in Porous Particles Packed in a Chromatographic Column. *J. Chromatogr. A* **1999**, *852*, 3–23.
- (21) Sadeghi, M. A.; Aghighi, M.; Barralet, J.; Gostick, J. T. Pore Network Modeling of Reaction-Diffusion in Hierarchical Porous Particles: The Effects of Microstructure. *Chem. Eng. J.* **2017**, *330*, 1002–1011.
- (22) Chen, L.; Zhang, R.; Min, T.; Kang, Q.; Tao, W. Pore-Scale Study of Effects of Macroscopic Pores and their Distributions on Reactive Transport in Hierarchical Porous Media. *Chem. Eng. J.* **2018**, *349*, 428–437.
- (23) Schneider, D.; Kondrashova, D.; Valiullin, R.; Bunde, A.; Kärger, J. Mesopore-Promoted Transport in Microporous Materials. *Chem. Ing. Tech.* **2015**, *87*, 1794–1809.
- (24) Schneider, D.; Mehlhorn, D.; Zeigermann, P.; Kärger, J.; Valiullin, R. Transport Properties of Hierarchical Micro–Mesoporous Materials. *Chem. Soc. Rev.* **2016**, *45*, 3439–3467.
- (25) Coasne, B.; Galarneau, A.; Gerardin, C.; Fajula, F.; Villemot, F. Molecular Simulation of Adsorption and Transport in Hierarchical Porous Materials. *Langmuir* **2013**, *29*, 7864–7875.
- (26) Tallarek, U.; Hlushkou, D.; Rybka, J.; Hölzel, A. Multiscale Simulation of Diffusion in Porous Media: From Interfacial Dynamics to Hierarchical Porosity. *J. Phys. Chem. C* **2019**, *123*, 15099–15112.
- (27) Gritti, F.; Guiochon, G. Theoretical Investigation of Diffusion along Columns Packed with Fully and Superficially Porous Particles. *J. Chromatogr. A* **2011**, *1218*, 3476–3488.
- (28) Gritti, F.; Guiochon, G. Diffusion Models in Chromatographic Columns Packed with Fully and Superficially Porous Particles. *Chem. Eng. Sci.* **2011**, *66*, 3773–3781.
- (29) Barrande, M.; Bouchet, R.; Denoyel, R. Tortuosity of Porous Particles. *Anal. Chem.* **2007**, *79*, 9115–9121.
- (30) Cernak, S.; Schuerholz, F.; Kespe, M.; Nirschl, H. Three-Dimensional Numerical Simulations on the Effect of Particle Porosity of Lithium-Nickel–Manganese–Cobalt–Oxide on the Performance of Positive Lithium-Ion Battery Electrodes. *Energy Technol.* **2021**, *9*, 2000676.
- (31) Birkholz, O.; Kamlah, M. Electrochemical Modeling of Hierarchically Structured Lithium-Ion Battery Electrodes. *Energy Technol.* **2021**, *9*, 2000910.
- (32) Naumann, J.; Bohn, N.; Birkholz, O.; Neumann, M.; Müller, M.; Binder, J. R.; Kamlah, M. Morphology-Dependent Influences on the Performance of Battery Cells with a Hierarchically Structured Positive Electrode. *Batteries Supercaps* **2023**, *6*, No. e202300264.
- (33) Neumann, M.; Stenzel, O.; Willot, F.; Holzer, L.; Schmidt, V. Quantifying the Influence of Microstructure on Effective Conductivity and Permeability: Virtual Materials Testing. *Int. J. Solids Struct.* **2020**, *184*, 211–220.
- (34) Neumann, M.; Wetterauer, S. E.; Osenberg, M.; Hilger, A.; Gräfensteiner, P.; Wagner, A.; Bohn, N.; Binder, J. R.; Manke, I.; Carraro, T.; Schmidt, V. A Data-Driven Modeling Approach to Quantify Morphology Effects on Transport Properties in Nanostructured NMC Particles. *Int. J. Solids Struct.* **2023**, *280*, 112394.
- (35) Birkholz, O.; Neumann, M.; Schmidt, V.; Kamlah, M. Statistical Investigation of Structural and Transport Properties of Densely-Packed Assemblies of Overlapping Spheres Using the Resistor Network Method. *Powder Technol.* **2021**, *378*, 659–666.
- (36) Kang, S. D.; Kuo, J. J.; Kapate, N.; Hong, J.; Park, J.; Chueh, W. C. Galvanostatic Intermittent Titration Technique Reinvented: Part II. Experiments. *J. Electrochem. Soc.* **2021**, *168*, 120503.
- (37) Dolotko, O.; Senyshyn, A.; Mühlbauer, M.; Nikolowski, K.; Ehrenberg, H. Understanding Structural Changes in NMC Li-Ion Cells by In Situ Neutron Diffraction. *J. Power Sources* **2014**, *255*, 197–203.
- (38) Kondrakov, A. O.; Schmidt, A.; Xu, J.; Geßwein, H.; Mönig, R.; Hartmann, P.; Sommer, H.; Brezesinski, T.; Janek, J. Anisotropic Lattice Strain and Mechanical Degradation of High- and Low-Nickel NCM Cathode Materials for Li-Ion Batteries. *J. Phys. Chem. C* **2017**, *121*, 3286–3294.
- (39) de Biasi, L.; Kondrakov, A. O.; Geßwein, H.; Brezesinski, T.; Hartmann, P.; Janek, J. Between Scylla and Charybdis: Balancing Among Structural Stability and Energy Density of Layered NCM Cathode Materials for Advanced Lithium-Ion Batteries. *J. Phys. Chem. C* **2017**, *121*, 26163–26171.
- (40) Strauss, F.; de Biasi, L.; Kim, A.-Y.; Hertle, J.; Schweidler, S.; Janek, J.; Hartmann, P.; Brezesinski, T. Rational Design of Quasi-Zero-Strain NCM Cathode Materials for Minimizing Volume Change Effects in All-Solid-State Batteries. *ACS Mater. Lett.* **2020**, *2*, 84–88.
- (41) Wu, S.-L.; Zhang, W.; Song, X.; Shukla, A. K.; Liu, G.; Battaglia, V.; Srinivasan, V. High Rate Capability of Li(Ni_{1/3}Mn_{1/3}Co_{1/3})O₂ Electrode for Li-Ion Batteries. *J. Electrochem. Soc.* **2012**, *159*, A438–A444.
- (42) Zahnw, J.; Bernges, T.; Wagner, A.; Bohn, N.; Binder, J. R.; Zeier, W. G.; Elm, M. T.; Janek, J. Impedance Analysis of NCM Cathode Materials: Electronic and Ionic Partial Conductivities and the Influence of Microstructure. *ACS Appl. Energy Mater.* **2021**, *4*, 1335–1345.
- (43) Hashin, Z.; Shtrikman, S. A Variational Approach to the Theory of the Elastic Behaviour of Multiphase Materials. *J. Mech. Phys. Solids* **1963**, *11*, 127–140.